

Molecular dynamics investigation of the structural and thermodynamic properties of gold nanoclusters of different morphologies

Yu Hang Chui,* Gregory Grochola, Ian K. Snook, and Salvy P. Russo

Applied Physics, School of Applied Science, RMIT University, GPO Box 2476 V, Melbourne, VIC, 3001, Australia

(Received 12 April 2006; published 8 January 2007)

Gold nanoclusters in the size range of 3–8 nm in diameter (923–10179) atoms were studied using the embedded atom method (EAM) “glue” potential. Three common structural morphologies for gold nanoclusters were considered: Icosahedral, defected icosahedral, and amorphous. The clusters were structurally relaxed and then analyzed by a structure measure technique using planar graphs. The free energies for the different cluster morphologies are also predicted as a function of cluster size. We show that glue potential can correctly predict the most stable structures observed in experiments from molecular dynamics simulations within the nanocluster size range we considered and that the effect of surface disorder is important in considering the stability of the nanoclusters.

DOI: 10.1103/PhysRevB.75.033404

PACS number(s): 61.46.Df

The stability of gold nanoclusters has been a subject of many experimental and theoretical studies recently.^{1–4} Many of the theoretical studies of gold nanoclusters have focused on calculating the total internal (or configurational) energy of the cluster as a means of assessing relative stability.^{5–7} In this study we use molecular dynamics (MD) and a robust structure measure criterion to compare the structure and stability of 923, 1415, 3871, and 10179 atom gold nanoclusters of three different morphologies (i) perfect icosahedrons, (ii) defected icosahedron-like nanoclusters, and (iii) amorphous nanoclusters, both the defected icosahedral and amorphous nanoclusters were quenched from the melt. All structures were generated by an icosahedron generation program.⁸ Using MD, clusters quenched from the melt were initially heated to 1400 K until a liquid-state equilibrium was achieved (after ~ 1.5 ns). To obtain the icosahedron-like nanoclusters we quenched to 298 K using three different cooling rates ($Q1=2 \times 10^{-11}$ s/K, $Q2=4 \times 10^{-11}$ s/K, and $Q3=6 \times 10^{-11}$ s/K) while the amorphous nanoclusters were formed by a one step quench to 298 K. The perfect icosahedral clusters were held at 298 K throughout the MD simulations. Once at 298 K, structures were equilibrated for 1 ns before analyzing their properties. All MD simulations were performed using the EAM glue potential^{3,5–7} with a time step of 5 fs. The glue potential uses the embedded atom method (EAM) formalism. The total energy is given by

$$E_{tot} = \sum_i F_i(\rho_h, i) + \frac{1}{2} \sum_{\substack{i,j \\ i \neq j}} \Phi_{ij}(R_{ij}), \quad (1)$$

where Φ_{ij} is the pair potential and F_i is an embedding term which models electronic interaction between gold atoms. Surface energy and transverse phonon frequency at the X point were included in fitting the potential, in order to describe both surface and bulk properties correctly.

We have chosen the glue potential as it gives a correct prediction of a number of surface properties and is able to predict the surface reconstruction, which is in good agreement with experimental findings.⁹ Previous studies have indicated this potential can reasonably give results in line with experimental observations of gold nanoparticles.^{10–12} In ad-

dition, Wang *et al.*¹³ modeled the melting behavior of gold nanorods using the glue potential and their result agrees with the laser heating experiment of gold nanorods.¹⁴ Therefore we believe that the glue potential is able to describe correct qualitative behavior of gold of a different morphologies at nanoscale.

In considering the stability of the various nanoclusters we estimated the Gibbs free energy of the clusters. If we assume that the vibrational entropy forms the largest contribution to the entropy of the nanocluster then the Gibbs free energy is given by

$$G = U - TS_{vib} + PV, \quad (2)$$

where U is the total internal energy, S_{vib} is the vibrational entropy, and P , T , and V are pressure, temperature, and volume, respectively. For a nanocluster at equilibrium in an isolated vacuum environment, the pressure is very close to zero and the PV term is negligible.

Within the harmonic approximation, the vibrational entropy $S_{vib}(V)$ of a cluster is related to the vibrational density of states $g(V, \omega)$ by¹⁵

$$S_{vib}(V) = - \frac{\partial F_{vib}(V)}{\partial T} = 3Nk_b \int_0^\infty \left[\frac{\hbar\omega}{2k_bT} \coth \frac{\hbar\omega}{2k_bT} - \ln \left(2 \sinh \frac{\hbar\omega}{2k_bT} \right) \right] g(V, \omega) d\omega, \quad (3)$$

where N is equal to the number of atoms in a nanocluster; k_b is the Boltzmann constant with units of eV K⁻¹; T is the absolute temperature in Kelvin, and $g(V, \omega)$ is the total vibrational density of states (VDOS) for the structure at volume V , and gives the number of modes with frequency lying in the interval $(\omega, \omega + d\omega)$. The VDOS of the gold nanoclusters is obtained from the Fourier transform of the velocity autocorrelation function,¹⁶ which is obtained routinely from MD simulations.¹⁷ In order to validate our results we calculated the vibrational entropy of bulk gold and our result (shown in Table I) agrees with that of Wu.¹⁵

Table I gives the calculated internal energies, vibrational entropies, and free energies of the perfect icosahedral, amorphous, and quenched defected icosahedral nanoclusters in-

TABLE I. Internal energy, entropy and free energy of gold nanoclusters investigated in the study. Values for bulk gold calculated from glue and *ab initio* potentials are also included. AMOR refers to the amorphous clusters, *Q1*: quenched nanocluster with the cooling rate= 2×10^{-11} s/K, *Q2*: quenched nanocluster with the cooling rate= 4×10^{-11} s/K, *Q3*: quenched nanocluster with the cooling rate= 6×10^{-11} s/K.

Cluster	Internal energy (<i>U</i>) (eV/atom)	Entropy (<i>S</i>) (10^{-4} eV K $^{-1}$ /atom)	<i>TS</i> (eV/atom)	Free energy (eV/atom)
Ih 923	-3.385	2.502	0.0746	-3.460
AMOR Au923	-3.374	2.558	0.0762	-3.450
Au 923 <i>Q1</i>	-3.404	2.534	0.0755	-3.480
Au 923 <i>Q2</i>	-3.402	2.540	0.0757	-3.478
Au 923 <i>Q3</i>	-3.404	2.530	0.0754	-3.479
Ih 1415	-3.433	2.493	0.0743	-3.508
AMOR Au1415	-3.415	2.555	0.0761	-3.491
Au 1415 <i>Q1</i>	-3.445	2.511	0.0748	-3.520
Au 1415 <i>Q2</i>	-3.448	2.525	0.0752	-3.523
Au 1415 <i>Q3</i>	-3.446	2.527	0.0753	-3.521
Ih 3871	-3.518	2.475	0.0738	-3.592
AMOR Au3871	-3.482	2.549	0.0760	-3.558
Au 3871 <i>Q1</i>	-3.525	2.497	0.0744	-3.600
Au 3871 <i>Q2</i>	-3.525	2.500	0.0745	-3.600
Au 3871 <i>Q3</i>	-3.526	2.496	0.0744	-3.601
Ih 10179	-3.577	2.460	0.0733	-3.650
AMOR Au10179	-3.534	2.540	0.0757	-3.609
Au 10179 <i>Q1</i>	-3.581	2.479	0.0739	-3.655
Au 10179 <i>Q2</i>	-3.583	2.482	0.0740	-3.657
Au 10179 <i>Q3</i>	-3.584	2.468	0.0735	-3.658
Bulk Au (Glue) (Ref. 9)	-3.741	2.357	0.0702	-3.811
Bulk Au (DFT) (Ref. 15)	—	2.456	—	—

investigated in this study. From the table, we find several interesting trends: First, for all cluster sizes the amorphous clusters have the least negative internal energy, highest vibrational entropy, and highest free energy and are uniformly the least thermodynamically stable cluster configuration. Second, although the perfect icosahedral clusters have the lowest entropy (of all the cluster morphologies), their free energy is slightly higher than that for the *q1*, *q2*, and *q3* quenched defected icosahedral clusters, for all cluster sizes, effectively due to the difference in their internal energy contributions. If the growth of gold nanoclusters is a thermodynamically driven process, at equilibrium the defected ico-

hedral structures have the highest probability of formation, and these kinds of structures are clearly observed in experimental studies.²

In order to compare the contribution of vibrational entropy from the surface and nonsurface atoms we calculated the percentage of vibrational entropy coming from the surface atoms for one of our cluster morphologies (the *Q2*

TABLE II. Relative percentage of vibrational entropy coming from the surface for the *Q2* quenched nanoclusters.

Nanocluster	Percentage of surface atoms in a nanocluster (%)	Percentage of vibrational entropy coming from surface atoms (%)
Au923 <i>q2</i>	43.77	46.06
Au1415 <i>q2</i>	38.94	41.14
Au3871 <i>q2</i>	29.19	31.01
Au10179 <i>q2</i>	21.75	23.27

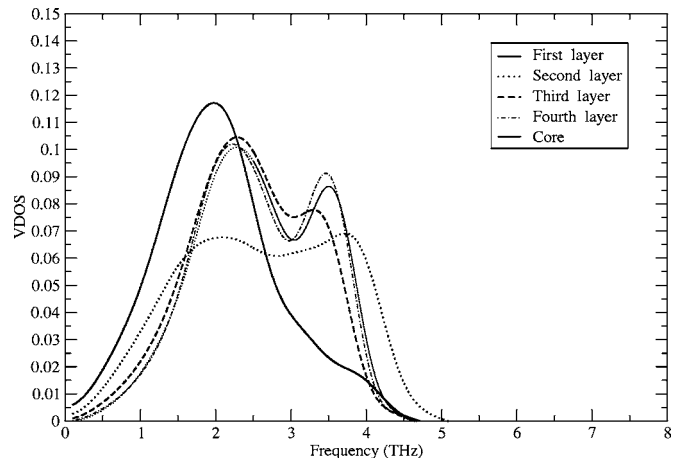


FIG. 1. Partial VDOS of different atomic layers and core zone for the *Q1* quenched Au10179 nanocluster.

TABLE III. A comparison of the vibrational entropy coming from the surface atoms of the perfect icosahedral (Ih) clusters and the Q2 quenched clusters.

Nanocluster	Entropy coming from the surface atoms in Ih nanocluster (S_{Ih}) (10^{-4} eV K/atom)	Entropy coming from the surface atoms in Q2 quenched nanoclusters (S_{Q2}) (10^{-4} eV K/atom)	Entropy difference ($S_{Q2} - S_{Ih}$) (10^{-4} eV K/atom)
Au923	2.68448	2.66562	-0.01886
Au1415	2.67522	2.66431	-0.01091
Au3871	2.67841	2.65535	-0.02306
Au10179	2.66558	2.65674	-0.00884

quenched clusters) and the results are given in Table II. The surface and nonsurface contributions to the vibrational entropy were obtained by projecting out their respective contributions to the total vibrational density of states. As an example, Fig. 1 shows the projected VDOS for the first 5 layers of the (Q1) quenched 10179 gold nanocluster. The figure indicates that the major contribution to the low frequency peak in the VDOS spectrum is due to surface phonon vibrations while the higher frequency peak is mainly due to bulklike phonons. Our VDOS results are consistent with those of Sun *et al.*¹⁸ who have performed similar analysis on the surface and bulk VDOS for smaller gold nanoclusters. In their study, Sun *et al.* gave the VDOS for Au 887 and Au 969

atom clusters for different regions (surface, transition shell, and core regions) and the transition in the VDOS distribution from low frequency (surface) modes to higher frequency (bulk) modes is also seen in our Fig. 1, where the cluster size is an order of magnitude larger.

From Table II we find that the percentage of vibrational entropy coming from the surface atoms is almost directly proportional to the percentage of surface atoms in the nanoclusters. In Table III, we compare the vibrational entropy coming from the surface atoms of the perfect and Q2 quenched icosahedral clusters. We find that the surface disorder in the Q2 quenched nanoclusters results in a lower vibrational entropy, compared to that of the perfect Ih nanoclusters. The disorder may help to reduce the surface strain

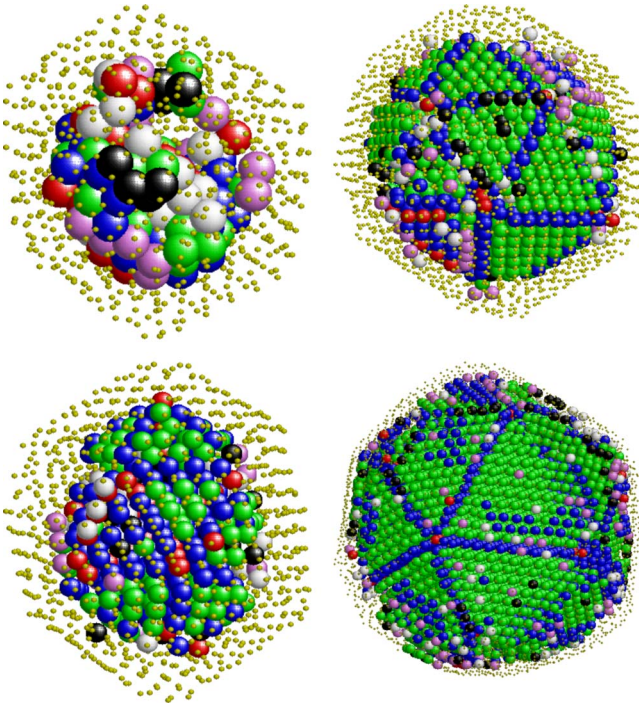


FIG. 2. (Color online) Classification of the core particles at (a) Q1 Au923 (top left), (b) Q1 Au1415 (bottom left), (c) Q1 Au3871 (top right), (d) Q1 Au10179 (bottom right). The colors of the core particles correspond to their topological classification based on planar graphs, green FCC, blue HCP, black defected FCC, gray defected HCP, red Ih, and twisted Ih, violet-stacking fault. The surface atoms are labeled in yellow with small radii.

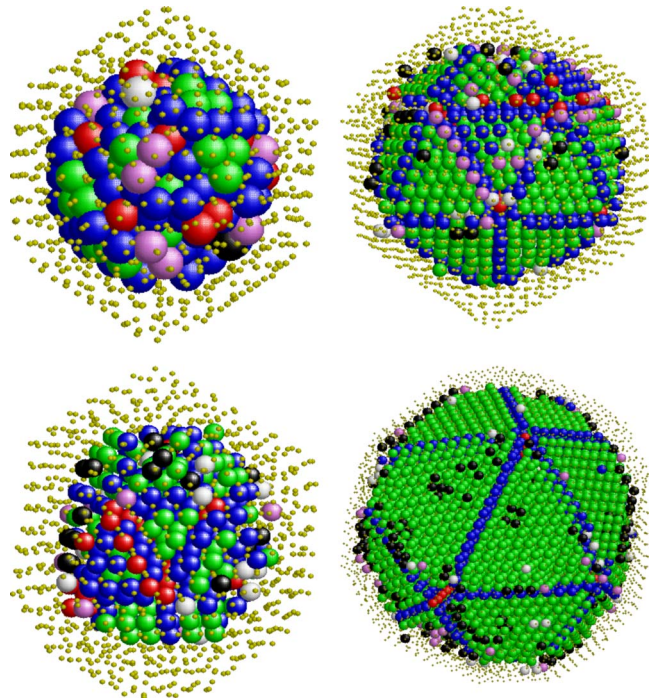


FIG. 3. (Color online) Classification of the core particles at (a) Q3 Au923 (top left), (b) Q3 Au1415 (bottom left), (c) Q3 Au3871 (top right), (d) Q3 Au10179 (bottom right). The colors of the core particles correspond to their topological classification based on planar graphs, green FCC, blue HCP, black defected FCC, gray defected HCP, red Ih, and twisted Ih, violet-stacking fault. The surface atoms are labeled in yellow with small radii.

of large icosahedral nanoclusters and stabilize the surface. Our findings here also agree with the fact that ideal icosahedral clusters consist of 20 (111) planes and surface reconstruction of (111) gold surfaces has been found to be energetically favorable from both experimental¹⁹ and theoretical studies.²⁰

In considering the morphological structure of the gold nanoclusters it is difficult to base any conclusion of the structure of the core on visual inspection of the cluster. In addition, common theoretical methods used to probe the structure of formed clusters, the radial distribution function (RDF), and bond-angle distribution function (BADF) can only provide a spatial average of the local environment of individual atoms. We have described elsewhere,²¹ a quantitative method for analyzing the ordering in the core of a cluster by describing the local environment of each particle using a classification scheme based on planar graphs.

A planar graph is a set of vertices (particles) joined by lines (bond between neighbors) such that no two lines cross one another. In this method, two particles are regarded as being bonded if their distance is less than or equal to the first minimum of the radial distribution function. Hence bonds are defined geometrically rather than chemically. The detailed definition of planar graphs can be found in Refs. 21 and 22.

Using our planar graph classification scheme we have analyzed the ordering of the gold cluster cores. Figures 2 and 3 show the classification of the core particles in the fastest (*Q1*, Fig. 2) and slowest (*Q3*, Fig. 3) quenched nanoclusters at 298 K. The colors of the particles correspond to their topological classification based on planar graphs (see figure captions for details). From the figures, we found that the hexagonal close packed (HCP) planes and face centered cubic (FCC) fragments in fivefold symmetry are clearly ob-

served in the Au₃₈₇₁ and Au₁₀₁₇₉ nanoclusters. In contrast, only small and disordered FCC and HCP local structures are found in the Au₉₂₃ and Au₁₄₁₅ nanoclusters. Figures 2 and 3 also show that the quench rate affects the disorder in the larger nanocluster cores. For the Au₃₈₇₁ and Au₁₀₁₇₉ nanoclusters, more well-ordered planes and fragments are formed in slowly quenched (*Q3*) nanoclusters. The effect of quench rate on structure is not significant in smaller nanoclusters. Fivefold symmetry can be clearly observed in 3871 and 10 179 atom nanoclusters, and this result is supported by the recent high resolution transmission electron microscopy (HRTEM) work of gold nanoclusters in helium gas by Koga *et al.*² In their studies Koga found that the icosahedral motif was the dominant one within the size range of our larger clusters (3.5–8 nm), while the other common motifs, such as fcc and decahedral structures, were nearly absent. Comparison of the experimental results of Koga *et al.* with our findings suggests that EAM glue potential provides a good unified description of the bulk, defect, and surface of gold.²³ This potential can correctly predict the most stable structures from molecular dynamics simulations within the nanocluster size range we considered. In contrast to the glue potential, the original EAM potential predicted the decahedral and even octahedral structures are the most stable with less than 500 atoms in a nanocluster.⁴

The authors would like to thank Peter Bath for assistance in calculating vibrational spectra and entropy. This project has been supported by the Victorian Partnership for Advanced Computing (VPAC) and the Australian Partnership for Advanced Computing (APAC). One of the authors (Y.H.C.) would also like to thank RMIT University for its financial assistance.

*Corresponding author. Email address: david.chui@rmit.edu.au

¹A. R. Sandy, S. G. J. Mochrie, D. M. Zehner, K. G. Huang, and D. Gibbs, *Phys. Rev. B* **43**, 4667 (1991).

²K. Koga and K. Sugawara, *Surf. Sci.* **529**, 23 (2003); K. Koga, T. Ikeshoji, and K. I. Sugawara, *Phys. Rev. Lett.* **92**, 115507 (2004).

³Y. Wang, S. Teitel, and C. Dellago, *Chem. Phys. Lett.* **394**, 257 (2004).

⁴C. L. Cleveland, W. D. Luedtke, and U. Landman, *Phys. Rev. B* **60**, 5065 (1999).

⁵F. Ercolessi, W. Andreoni, and E. Tosatti, *Phys. Rev. Lett.* **66**, 911 (1991).

⁶B. Wang, S. Yin, G. Wang, A. Buldum, and J. Zhao, *Phys. Rev. Lett.* **86**, 2046 (2001).

⁷Y. Wang and C. Dellago, *J. Phys. Chem. B* **107**, 9214 (2003).

⁸Available at <http://www.pas.rochester.edu/~wangyt/algorithms/index.html>

⁹F. Ercolessi, M. Parrinello, and E. Tosatti, *Philos. Mag. A* **58**, 213 (1988).

¹⁰F. Ercolessi, W. Andreoni, and E. Tosatti, *Phys. Rev. Lett.* **66**, 911 (1991).

¹¹Y. Wang, S. Teitel, and C. Dellago, *Chem. Phys. Lett.* **394**, 257 (2004).

¹²B. Wang, S. Yin, G. Wang, A. Buldum, and J. Zhao, *Phys. Rev.*

Lett. **86**, 2046 (2001).

¹³Y. Wang and C. Dellago, *J. Phys. Chem. B* **107**, 9214 (2003).

¹⁴S. Link, C. Burda, B. Nikoobakht, and M. A. El-Sayed, *J. Phys. Chem. B* **104**, 7867 (2000).

¹⁵E. J. Wu, Ph.D. Thesis, Massachusetts Institute of Technology (2002). Available at <http://burgaz.mit.edu/PUBLICATIONS/theses.php>

¹⁶M. T. Dove, *Introduction to Lattice Dynamics* (Cambridge University Press, Cambridge, 1993).

¹⁷M. P. Allen and D. J. Tildesley, *Computer Simulation of Liquids* (Oxford University Press, New York, 1987), p. 232.

¹⁸D. Y. Sun, X. G. Gong, and X. Q. Wang, *Phys. Rev. B* **63**, 193412 (2001).

¹⁹U. Harten, A. M. Lahee, J. P. Toennies, and C. Wöll., *Phys. Rev. Lett.* **54**, 2619 (1985).

²⁰A. Bartolini, F. Ercolessi, and E. Tosatti, *The Structure of Surfaces II*, edited by J. F. van der Veen and M. A. Van Hove (Springer-Verlag, Berlin, 1988), p. 132.

²¹Y. H. Chui, R. Rees, I. K. Snook, B. O'Malley, and S. P. Russo, *J. Chem. Phys.* **125**, 114703 (2006).

²²B. O'Malley, Ph.D. thesis, RMIT (2001).

²³F. Ercolessi, M. Parrinello, and E. Tosatti, *Philos. Mag. A* **58**, 213 (1988).